

# Statics and Dynamics of an Inhomogeneously-Nonlinear Lattice

Debra L. Machacek<sup>1</sup>, Elizabeth A. Foreman<sup>1</sup>, Q.E. Hoq<sup>2</sup>,  
P.G. Kevrekidis<sup>1</sup>, A. Saxena<sup>3</sup>, D.J. Frantzeskakis<sup>4</sup> and A.R. Bishop<sup>3</sup>

<sup>1</sup> Department of Mathematics, University of Massachusetts, Amherst, Massachusetts, 01003-4515, USA

<sup>2</sup> Department of Mathematics, Western New England College, Springfield, MA, 01119, USA

<sup>3</sup> Theoretical Division and Center for Nonlinear Studies, Los Alamos National Laboratory, Los Alamos, NM 87545, USA

<sup>4</sup> Department of Physics, University of Athens, Panepistimiopolis, Zografos, Athens 15784, Greece

April 28, 2017

## Abstract

We introduce an inhomogeneously-nonlinear Schrödinger lattice, featuring a defocusing segment, a focusing segment and a transitional interface between the two. We illustrate that such inhomogeneous settings present vastly different dynamical behavior than the one expected in their homogeneous counterparts in the vicinity of the interface. We analyze the relevant stationary states, as well as their stability by means of perturbation theory and linear stability analysis. We find good agreement with the numerical findings in the vicinity of the anti-continuum limit. For larger values of the coupling, we follow the relevant branches numerically and show that they terminate at values of the coupling strength which are larger for more extended solutions. The dynamical development of relevant instabilities is also monitored in the case of unstable solutions.

## 1 Introduction

In the past two decades, the number of applications of discrete, nonlinear dynamical models has increased dramatically. A diverse set of applications has emerged, ranging from the nonlinear optics of guided waves in inhomogeneous optical structures [1, 2] and photonic crystal lattices [3, 4], to atomic physics and the dynamics of Bose-Einstein condensate (BEC) droplets in periodic (optical lattice) potentials [5, 6, 7, 8] and from condensed matter, in Josephson-junction ladders [9, 10], to biophysics, in various models of double-stranded DNA [11, 12]. This broad span of research areas and corresponding applications has now been summarized in a variety of reviews [13, 14, 15, 16, 17].

A model that has drawn a particular focus among these areas of applications is the so-called discrete nonlinear Schrödinger equation (DNLS) [16]. This model was first proposed in the context of nonlinear optics, where it describes beam dynamics in coupled waveguide arrays [18, 19], but is equally applicable in other settings, such as the dynamics of BECs confined in deep optical lattices [8, 20]. The relevant model involves the nearest neighbor coupling between adjacent waveguides

(wells of the optical lattice in BECs) and the local nonlinear self-action induced by the Kerr effect in each waveguide (or the mean-field inter-atomic interaction in the condensate setting).

Typically, the above setup is homogeneous in that all waveguides or wells are identical. However, recently there has been a surge of activity motivated by the experimental tunability of the properties of individual waveguides/wells. In particular, in the optical setting, the interaction of discrete solitary waves with structural defects was examined in [21], while “non-standard” solitary waves (discrete gap solitons) were observed in binary waveguide arrays [22, 23]. This activity has been recently reviewed in [24] discussing various aspects of “optics in non-homogeneous waveguide arrays”. On the BEC side, there are also similar developments involving not only the (attractive or repulsive) localized “defect” action of a laser beam on the condensate [25, 26], but also the potential of creating the so-called “superlattice” structures by means of the superposition of optical potentials of different periodicity [27].

In this context of inhomogeneous nonlinear dynamical systems, we propose here a novel setting, which we illustrate to have drastically different dynamical behavior than that we would expect from its homogeneous counterparts. In particular, we impose a spatial pattern on the nonlinearity, having the form of an “interface” between a set of defocusing Kerr waveguides on the one end and a set of focusing Kerr waveguides on the other, separated by a “transient” layer (interface) of a waveguide bearing intermediate properties between the two segments above. This is, in some aspects, reminiscent to the recent proposition in the context of BECs of spatially dependent nonlinearities (see e.g. [28, 29, 30] and references therein). We show that this setting already presents a wealth of static and dynamical behavior which is very different than its homogeneous analog.

We focus on the localized, solitary wave excitations in the vicinity of the interface. Starting from the so-called anti-continuum limit of zero coupling [31], we show that the existence and stability of the localized solutions in the vicinity of the interface can be quantified for low couplings by means of a perturbation theory using the coupling constant as small parameter. As the coupling between the sites near the interface increases, the phenomenology becomes drastically different, leading the relevant solution branches to a termination through saddle-node bifurcations that would be absent in the corresponding homogeneous limit. Perhaps equally surprisingly, the more extended multi-pulse solutions appear to survive for larger values of the coupling than the single (or smaller size) pulse waves, which is again contrary to what is expected from the homogeneous limit. In this stronger coupling regime, we investigate the properties of the relevant solutions through numerical bifurcation theory and linear stability analysis. We use direct numerical simulations to illustrate the manifestations of the dynamical instabilities of those among the solutions which are found to be dynamically unstable. We believe that this example illustrates the rich diversity of behavior that can be manifested in such inhomogeneous settings.

Our presentation is structured as follows: in section 2, we present the setup and analytical results, while in section 3, we study the model numerically and compare with the analytical results. Finally, in section 4, we summarize our findings and present our conclusions.

## 2 Setup and Analytical Results

We consider an inhomogeneous lattice model described by a discrete non-linear Schrödinger equation of the following form,

$$i\frac{du_n}{dt} = -C\Delta_2 u_n - d_n|u_n|^2 u_n, \quad (2.1)$$

where  $C$  is the coupling between the adjacent sites of the lattice,  $\Delta_2 u_n = (u_{n+1} + u_{n-1} - 2u_n)$  is the discrete Laplacian. The evolution variable is  $z$  in the optical case and  $t$  in the BEC case; for notational simplicity, we use  $t$  in what follows. The nonlinearity coefficient  $d_n$  (where  $n$  is the spatial index) is determined by the intensity-dependent refractive index (in the context of optics) or the s-wave scattering length (in the context of BECs) of each waveguide (or optical lattice well for BECs). The center site,  $d_0$ , is assumed to have an intermediate value slightly greater than zero. For all  $n < 0$ , the refractive index is set to the defocusing value  $d_n = -0.9$ . For all  $n > 0$ , the refractive index is set to the focusing value  $d_n = 1.1$ . Note that  $d_0$  is set to the average of these two values i.e., to 0.1; it should also be mentioned that the results reported below were found to be typical of similar choices of the  $d_n$  profile.

We focus our attention on standing wave solutions of the form of  $u_n = e^{i\Lambda t} v_n$ , where  $\Lambda$  is the propagation constant in optics or the chemical potential in BECs, and  $v_n$  is the spatial (time-independent) profile, satisfying the steady state equation:

$$G(v_n, C) \equiv \Lambda v_n - C\Delta_2 v_n - d_n|v_n|^2 v_n = 0. \quad (2.2)$$

It can be easily seen (see e.g. Refs. [32, 33]) that, without loss of generality, we can restrict ourselves to the class of real solutions of Eq. (2.2). In the anti-continuum (AC) limit, i.e., for  $C = 0$ , the solutions are immediately obtainable in the form:  $v_n^2 = \{0, \frac{\Lambda}{d_n}\}$ , provided that  $d_n > 0$  for all  $n$ . Using this solution and setting to non-zero values only specific individual sites to the right of the zeroth site, we prescribe the configurations (in the AC limit) for the various branches that will be subsequently examined analytically as well as numerically. The selected configurations are as follows; lower first branch  $|1\rangle$ : single excited site at  $n = 0$ ; upper first branch  $|1, e\rangle$ : excited sites at  $n = 0$  and  $n = 1$  in phase; lower second branch  $|1, -e\rangle$ : excited sites  $n = 0$  and  $n = 1$  but out of phase; upper second branch  $|1, -e, -e\rangle$ : excited sites  $n = 0$  with positive sign and  $n = 1, 2$  with negative signs. Following the same pattern, the remaining branches are: lower third branch  $|1, -e, e\rangle$ ; upper third branch  $|1, -e, e, e\rangle$ ; lower fourth branch  $|1, -e, e, -e\rangle$ ; upper fourth branch  $|1, -e, e, -e, -e\rangle$ ; lower fifth branch  $|1, -e, e, -e, e\rangle$ ; upper fifth branch  $|1, -e, e, -e, e, e\rangle$ .

On the numerical side, we analyse these branches using the pseudo-arclength continuation method [34]. This allows us to trace the branches past fold points. In particular, given a solution  $(\vec{v}_0, C_0)$  of the equation (2.2)  $G(\vec{v}, c) = 0$  and a direction vector  $(\vec{v}_0, \dot{C}_0)$ , one can determine  $(\vec{v}_1, C_1)$  by solving the following system of equations:

$$\begin{aligned} G(\vec{v}_1, C_1) &= 0, \\ (\vec{v}_1 - \vec{v}_0)\vec{v}_0 + (C_1 - C_0)\dot{C}_0 - \Delta s &= 0, \end{aligned} \quad (2.3)$$

where  $\Delta s$  is a (small) arclength parameter. We use Newton's method to solve the system in Eq. (2.3) for  $(\vec{v}_1, C_1)$ :

$$\begin{pmatrix} \frac{\partial}{\partial \vec{v}} G_1 & \frac{\partial}{\partial C} G_1 \\ \vec{v}_0 & \dot{C}_0 \end{pmatrix} \begin{pmatrix} \vec{v}_1 - \vec{v}_0 \\ C_1 - C_0 \end{pmatrix} = - \begin{pmatrix} G(\vec{v}_1, C_1) \\ (\vec{v}_1 - \vec{v}_0)\vec{v}_0 + (C_1 - C_0)\dot{C}_0 - \Delta s \end{pmatrix}. \quad (2.4)$$

The next (normalized) direction vector,  $(\vec{v}_1, \dot{C}_1)$ , can be computed by solving:

$$\begin{pmatrix} \frac{\partial}{\partial \vec{v}} G_1 & \frac{\partial}{\partial \dot{C}} G_1 \\ \vec{v}_0 & \dot{C}_0 \end{pmatrix} \begin{pmatrix} \vec{v}_1 \\ \dot{C}_1 \end{pmatrix} = \begin{pmatrix} 0 \\ 1 \end{pmatrix}. \quad (2.5)$$

To examine the linear stability of the stationary solutions obtained as described above, we use the perturbation ansatz

$$u_n = e^{i\Lambda t} (v_n + \epsilon a_n e^{-i\omega t} + b_n e^{i\omega^* t}), \quad (2.6)$$

where  $\epsilon$  is a formal small parameter. By substituting Eq. (2.6) into Eq. (2.1) and dropping higher order terms, the following system of linear stability equations is obtained:

$$\begin{aligned} \omega a_n &= -c\Delta_2 a_n + \Lambda a_n - 2d_n |v_n|^2 a_n - d_n v_n^2 b_n^*, \\ \omega^* b_n &= c\Delta_2 b_n - \Lambda b_n + 2d_n |v_n|^2 b_n + d_n v_n^2 a_n^*. \end{aligned} \quad (2.7)$$

The numerical solution of the ensuing matrix eigenvalue problem for the eigenfrequencies  $\omega$  and eigenvectors  $\{a_n, b_n^*\}$  can be then used to characterize the linear stability (more precisely the spectral stability) of the solutions. Since the eigenvalues (eigenfrequencies) of the underlying Hamiltonian system appear in quartets, to ensure a spectral instability it suffices for the above linear system to possess an eigenfrequency with a non-zero imaginary part. When the solutions are found to be unstable, we use a fourth-order, direct integration scheme to examine the dynamical evolution of the instability.

Having presented the main framework and numerical methods, we now turn to some analytical results. Our analysis will be based on perturbation theory from the anti-continuum limit, using the coupling strength  $C$  as the small parameter. In particular, we expand the solution as:

$$v_n = v_n^{(0)} + C v_n^{(1)} + O(C^2). \quad (2.8)$$

It is easy to check that the stability problem of Eq. (2.7) can be rewritten for the eigenvalues  $\lambda = i\omega$  in the Hamiltonian form

$$\mathcal{J}\mathcal{H}\psi = \lambda\psi, \quad (2.9)$$

where  $\psi$  is the infinite-dimensional eigenvector, consisting of 2-blocks of  $(u_n, w_n)^T$  (the superscript  $T$  denotes transpose), where  $a_n = u_n + iw_n$ ,  $b_n = u_n - iw_n$  for the eigenvector equations (2.7),  $\mathcal{J}$  is the infinite-dimensional skew-symmetric matrix, which consists of 2-by-2 blocks of

$$\mathcal{J}_{n,m} = \begin{pmatrix} 0 & 1 \\ -1 & 0 \end{pmatrix} \delta_{n,m},$$

and  $\mathcal{H}$  is the infinite-dimensional symmetric matrix, which consists of 2-by-2 blocks of

$$\mathcal{H}_{n,m} = \begin{pmatrix} (\mathcal{L}_+)_{n,m} & 0 \\ 0 & (\mathcal{L}_-)_{n,m} \end{pmatrix}.$$

The matrices  $(\mathcal{L}_+)_{n,m}$  and  $(\mathcal{L}_-)_{n,m}$  are, in turn, defined as:

$$(\mathcal{L}_+)_{n,n} = 1 - 3d_n v_n^2, \quad (\mathcal{L}_-)_{n,n} = 1 - d_n v_n^2, \quad (\mathcal{L}_\pm)_{n,n+1} = (\mathcal{L}_\pm)_{n+1,n} = -C.$$

Similarly to the solution itself, the matrix  $\mathcal{H}$  in the neighborhood of the AC limit, can be expanded as

$$\mathcal{H} = \mathcal{H}^{(0)} + \sum_{k=1}^{\infty} C^k \mathcal{H}^{(k)}, \quad (2.10)$$

where  $\mathcal{H}^{(0)}$  is diagonal with two blocks:

$$\mathcal{H}_{n,n}^{(0)} = \begin{pmatrix} -2 & 0 \\ 0 & 0 \end{pmatrix}, \quad n \in S, \quad \mathcal{H}_{n,n}^{(0)} = \begin{pmatrix} 1 & 0 \\ 0 & 1 \end{pmatrix}, \quad n \in \mathbb{Z} \setminus S, \quad (2.11)$$

where  $S$  denotes the set of excited sites. Notice that in the  $C = 0$  limit, each excited site corresponds to a pair of zero eigenvalues in equation (2.9), while each zero-site corresponds to a pair of eigenvalues at  $\pm 1$ .

Choosing for simplicity of exposition (and without loss of generality)  $\Lambda + 2C = 1$  in Eq. (2.2), the solution of the leading perturbation problem in (2.8) is governed by the following equation:

$$[1 - 3d_n(v_n^{(0)})^2]v_n^{(1)} = v_{n+1}^{(0)} + v_{n-1}^{(0)}. \quad (2.12)$$

One can apply this, e.g., for the 2-site solutions such as  $|1, e\rangle$  and  $|1, -e\rangle$ , to obtain the leading order corrections:

$$v_0^{(1)} = -\frac{1}{2}(\pm\sqrt{\frac{1}{d_1}}), \quad (2.13)$$

$$v_1^{(1)} = -\frac{1}{2}(\pm\sqrt{\frac{1}{d_0}}), \quad (2.14)$$

where the sign inside the parenthesis corresponds to the sign of excitation of the site indexed inside the square root. Similarly, for 3 excited sites the expressions become

$$v_0^{(1)} = -\frac{1}{2}(\pm\sqrt{\frac{1}{d_1}}), \quad (2.15)$$

$$v_1^{(1)} = -\frac{1}{2}(\pm\sqrt{\frac{1}{d_0}} \pm \sqrt{\frac{1}{d_2}}), \quad (2.16)$$

$$v_2^{(1)} = -\frac{1}{2}(\pm\sqrt{\frac{1}{d_1}}). \quad (2.17)$$

One can correspondingly generalize these expressions for an arbitrary number of excited sites.

We now turn to the perturbed stability problem. The small perturbation of size  $C$  cannot render the eigenvalues of order  $O(1)$  unstable. Instead, the potentially “dangerous” eigenvalues for instability purposes are those which are located at the origin of the spectral plane in the AC limit (corresponding to the excited sites, as discussed above). The perturbed form  $\mathcal{H}_1$  of the matrix relevant to the stability problem can be easily seen (from the perturbative expansion) to assume the form

$$\mathcal{H}_{n,n}^{(1)} = -2d_n\phi_n^{(0)}\phi_n^{(1)} \begin{pmatrix} 3 & 0 \\ 0 & 1 \end{pmatrix}, \quad \mathcal{H}_{n,n+1}^{(1)} = \mathcal{H}_{n+1,n}^{(1)} = - \begin{pmatrix} 1 & 0 \\ 0 & 1 \end{pmatrix}, \quad (2.18)$$

while all other blocks of  $\mathcal{H}_{n,m}^{(1)}$  are zero. If we consider the (linearly independent) eigenvectors corresponding to zero eigenvalues of  $\mathcal{H}_0$ ,  $\mathbf{f}_n$ , then it was proved in [33] that in order to obtain the leading correction to the (zero) eigenvalues of the original problem, it is sufficient to consider the reduced problem

$$\mathcal{M}_1 \mathbf{c} = \gamma_1 \mathbf{c}, \quad (2.19)$$

where

$$(\mathcal{M}_1)_{m,n} = (\mathbf{f}_m, \mathcal{H}^{(1)} \mathbf{f}_n) \quad (2.20)$$

is an  $N \times N$  matrix, with  $N$  being the number of excited sites. Once the eigenvalues  $\gamma_1$  of this reduced problem are obtained, then the perturbed eigenvalues of the original problem are given by the form  $\lambda = \sqrt{C}\lambda_1 + O(C)$ , where  $\lambda_1 = \sqrt{2\gamma_1}$ .

One can then directly compute the matrix  $\mathcal{M}$ , e.g. in the 2-site and 3-site cases, as well as more generally, to have the forms

$$(\mathcal{M})_{n,n} = -2d_n v_n^{(0)} v_n^{(1)}, \quad (\mathcal{M})_{n,n-1} = -\cos(\theta_{n-1} - \theta_n), \quad (\mathcal{M})_{n,n+1} = -\cos(\theta_{n+1} - \theta_n).$$

One can then obtain the following predictions for the leading order eigenvalues of some of the branches discussed above (we only explicitly present these predictions in the 2- and 3-site cases)

$$\lambda = \pm 2.69003\sqrt{C}, \quad (2.21)$$

$$\lambda = \pm 2.69003i\sqrt{C}, \quad (2.22)$$

for the (unstable)  $|1, e\rangle$  and (stable, at least for small  $C$ )  $|1, -e\rangle$  modes, respectively. In the 3-site, we have:

- For the branch  $|1, e, e\rangle$ , two real eigenvalue pairs:

$$\lambda_1 = \pm 1.277714\sqrt{C}, \quad \lambda_2 = \pm 3.098986\sqrt{C}; \quad (2.23)$$

- For the branch  $|1, -e, e\rangle$ , the same eigenvalue pairs as above but multiplied by  $i$  (hence the branch is marginally stable for small  $C$ );
- For the branch  $|1, e, -e\rangle$ , one real and one imaginary pair in the form:

$$\lambda_1 = \pm 1.63075i\sqrt{C}, \quad \lambda_2 = \pm 2.428092\sqrt{C}; \quad (2.24)$$

- Similarly, the branch  $|1, -e, -e\rangle$  has the same eigenvalues as  $|1, e, -e\rangle$  but multiplied by  $i$  (so it is also always linearly unstable).

Notice that one can, in principle, expand this type of analysis to any other configuration of interest. We now turn to numerical results in order to examine the validity of these theoretical predictions.

### 3 Numerical Results

Figure 1 summarizes our essential numerical results, presenting the squared  $l^2$  norm of the solution (physically, the power in optics or the rescaled number of atoms in BEC)  $P = \sum_n |u_n|^2$  for the various branches that we examined in our computations. [For the explanation of the branches that are shown, the reader is referred to section 2]. There is a number of features in this bifurcation diagram which are in extreme contrast with the corresponding homogeneous limit of this system. Firstly, the single pulse branch in the vicinity of the interface already terminates for quite small values of  $C$ ; in fact, it is the first branch to terminate in a saddle-node bifurcation with the two-site mode  $|1, e\rangle$ . This is the analog of what would be termed “the Page mode” in the setting of intrinsic localized modes (ILMs). As the coupling increases, the site with index  $n = 1$  starts becoming excited for the single pulse branch eventually colliding (in configuration space) with the 2-site mode and

annihilating each other. In the homogeneous limit of a focusing medium both of these branches would survive for *any*  $C$ , up to the continuum limit of  $C \rightarrow \infty$ . A similar phenomenology emerges for the so-called twisted mode branch of  $|1, -e \rangle$  that, in turn, is also linearly stable for small  $C$ ; for larger  $C$  it eventually collides with the branch  $|1, -e, -e \rangle$  and disappears in a saddle-node bifurcation. The same is also true for the pair of  $|1, -e, e \rangle$  and  $|1, -e, e, e \rangle$  and for that of  $|1, -e, e, -e \rangle$  and  $|1, -e, e, -e, -e \rangle$  also shown in the figure. Another interesting general trend illustrated in this diagram is that the more extended the branch (i.e., the more sites participating in the nonlinear wave), the larger the coupling strength for which it persists. This is also contrary to what one would expect from the homogeneous limit, where multi-site solutions can only be continued to a finite coupling which is typically larger for more localized structures.

Figure 2 illustrates the details of the lower pair of branches in Fig. 1. In particular, the top left panel shows the profile of the modes and their corresponding stability for the stable  $|1 \rangle$  and unstable  $|1, e \rangle$  solutions. The continuation of the branches (up to  $C = 0.15$  where they collide and disappear) is shown in detail. The instability of the unstable two-site solution is investigated in the right panel through a direct simulation showing its breathing evolution. Panel (c) reports the result of the full numerical simulation (solid line) versus the theoretical prediction (dashed line), both for the instability eigenvalue of  $|1, e \rangle$ , and the profile correction imposed by Eqs. (2.13)-(2.14). It is readily observed that, for small values of  $C$ , the agreement between the analytical predictions and the numerical results is very good. Of course, for larger  $C$ , the analytical results are expected to be less successful due to the significance of higher-order corrections neglected in our analysis.

Figure 3 is similar to Fig. 2, but for the second pair of solutions in Fig. 1, namely for  $|1, -e \rangle$  and its corresponding unstable companion  $|1, -e, -e \rangle$ . These branches disappear together in a saddle-node bifurcation for  $C = 0.575$ . While  $|1, -e, -e \rangle$  is always unstable due to a real eigenvalue for any  $C$ , the twisted mode is stable for small  $C$ , but becomes unstable for  $C > 0.095$  due to the collision of two imaginary eigenvalue pairs with opposite Krein signature, leading to a quartet of eigenvalues through a Hamiltonian Hopf bifurcation [35]. The top left panel of the figure illustrates the solution profiles, the bifurcation diagram, and the results of the stability analysis. The top right highlights the breathing evolution of the twisted mode state. The two bottom panels compare the eigenvalue prediction of Eq. (2.22) with the full numerical result (dashed vs. solid lines) and the leading order correction for the two side mode, in the case of the left panel. In the right panel, the eigenvalue predictions (one real and one imaginary) for the  $|1, -e, -e \rangle$  branch (dashed line) are also compared to the corresponding numerical results (solid line), obtaining once again good agreement.

In Figure 4, we examine the third pair of branches of Fig. 1, namely (the stable for small  $C$ )  $|1, -e, e \rangle$  and (the always unstable)  $|1, -e, e, e \rangle$ . These branches, in turn, collide and disappear through a saddle-node for  $C = 0.725$ . The top right panel shows the prediction (dashed line) versus the numerical results (solid line) for the leading order eigenvalues of the  $|1, -e, e \rangle$  solution (discussed in the previous section). The theory correctly captures, at small  $C$ , the existence of two imaginary eigenvalues and their  $C^{1/2}$  bifurcation from 0, but is somewhat less satisfactory quantitatively in this case. This branch becomes unstable around  $C = 0.08$  due to the collision of one of these eigenvalue pairs with one of opposite Krein signature, leading once again to a quartet of eigenvalues. The details of the subsequent dependence of this unstable eigenvalue on  $C$ , both for this branch and for  $|1, -e \rangle$ , depend also on this size of the domain for reasons similar to

those discussed in [36]. The two bottom panels show the unstable evolution of the corresponding solutions, illustrating an interesting phenomenon particularly in the case of the  $|1, -e, e >$  branch. The dynamical evolution favors the tunneling of the excitation from the position of the interface to a nearby site (in this case, mainly to  $n = 2$ ). That is, the interface displaces the solution towards a position where the environment is more conducive (being surrounded by focusing sites) to the existence of a localized pulse solution.

## 4 Conclusions

In the present paper, we have introduced a new setting for the study of the recent theme of inhomogeneous nonlinear lattices in nonlinear optics (waveguide arrays) and Bose-Einstein condensates (optical lattices and superlattices). The setting consists of an interface between defocusing and focusing (repulsive interaction and attractive interaction, respectively) regions and a transient layer between the two.

We have focused specifically on the statics and dynamics of coherent waveforms in the vicinity of this interface, and we have found that their properties are dramatically modified in comparison with those expected from the homogeneous case. Some manifestations of these differences can be quantified in the termination of the principal pulse branch (for small couplings) or the more prolonged (in parameter space) persistence of more extended structures in comparison with more localized ones. Furthermore, we have shown that the interface may induce a dynamical tunneling of the structures towards locations more favorable for their existence. We have also developed a systematic methodology based on the adaptation of the considerations of [33] to inhomogeneous settings and illustrated how to use these to develop a perturbative treatment of the problem with excellent qualitative and good quantitative agreement with the full numerical results.

There are many interesting questions that are suggested for the interface problem we have introduced. A prominent one concerns the dynamical evolution of localized structures towards the interface and their interaction (transmission, reflection or trapping) with that region.



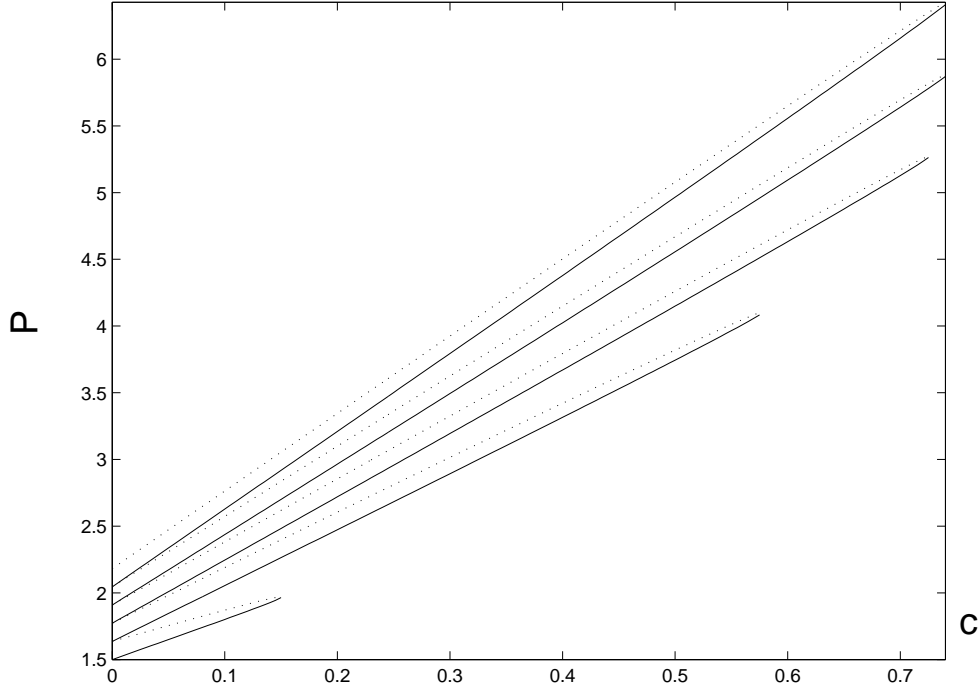


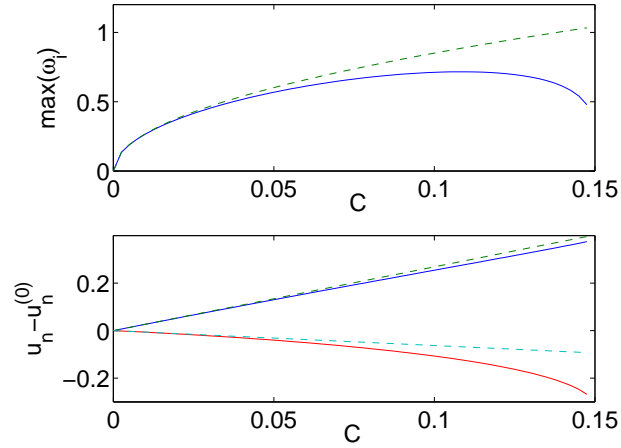
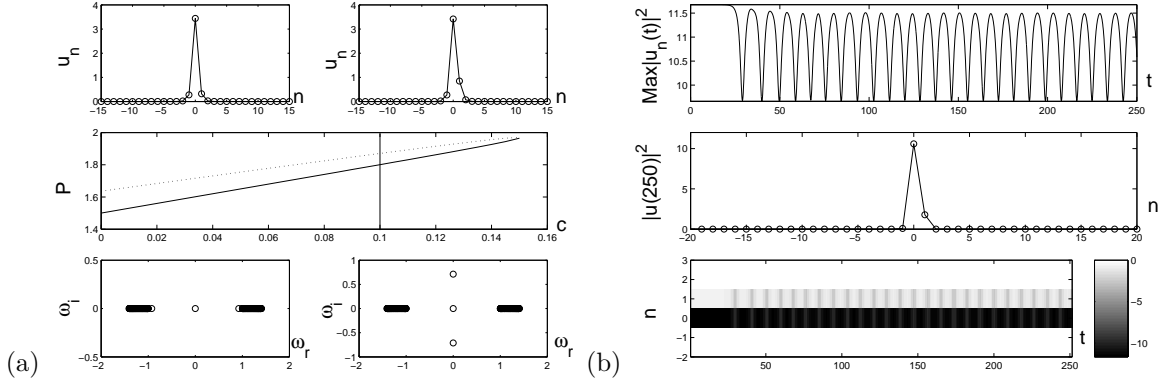
Figure 1: Bifurcation diagram of the first five branches. Plot of the solution's power vs. the continuation parameter,  $C$ . Dotted lines represent unstable regions. Solid lines represent initially stable regions.

## References

- [1] H.S. Eisenberg, R. Morandotti, Y. Silberberg, J.M. Arnold, G. Pennelli, and J.S. Aitchison, *J. Opt. Soc. Am. B* **19**, 2938 (2002).
- [2] U. Peschel, R. Morandotti, J.M. Arnold, J.S. Aitchison, H.S. Eisenberg, Y. Silberberg, T. Pertsch, and F. Lederer, *J. Opt. Soc. Am. B* **19**, 2637 (2002).
- [3] N.K. Efremidis, S. Sears, D.N. Christodoulides, J.W. Fleischer, and M. Segev, **66**, 046602 (2002).
- [4] A.A. Sukhorukov, Yu.S. Kivshar, H.S. Eisenberg, and Y. Silberberg, *IEEE J. Quantum Elect.* **39**, 31 (2003).
- [5] F.S. Cataliotti, S. Burger, C. Fort, P. Maddaloni, F. Minardi, A. Trombettoni, A. Smerzi, and M. Inguscio, *Science* **293**, 843 (2001).
- [6] F.S. Cataliotti, L. Fallani, F. Ferlaino, C. Fort, P. Maddaloni, and M. Inguscio, *New. J. Phys.* **5**, 71 (2003).
- [7] F.Kh. Abdullaev, B.B. Baizakov, S.A. Darmanyan, V.V. Konotop, and M. Salerno, *Phys. Rev. A* **64**, 043606 (2001).
- [8] G.L. Alfimov, P.G. Kevrekidis, V.V. Konotop, and M. Salerno, *Phys. Rev. E* **66**, 046608 (2002).

- [9] M.V. Fistul, Chaos **13**, 725 (2003).
- [10] J.J. Mazo and T.P. Orlando, Chaos **13**, 733 (2003).
- [11] T. Dauxois, M. Peyrard and A.R. Bishop, Phys. Rev. E **47**, R44 (1993).
- [12] M. Peyrard, T. Dauxois, H. Hoyet, and C.R. Willis, Physica D **68**, 104 (1993).
- [13] S. Aubry, Physica D **103**, 201 (1997).
- [14] S. Flach and C.R. Willis, Physics Reports **295**, 181 (1998).
- [15] D. Hennig and G. Tsironis, Physics Reports **307**, 333 (1999).
- [16] P.G. Kevrekidis, K.O. Rasmussen, and A.R. Bishop, Int. J. Mod. Phys. B **15**, 2833 (2001).
- [17] J.Ch. Eilbeck and M. Johansson, in *Localization and Energy Transfer in Nonlinear Systems*, L. Vazquez, R.S. MacKay, and M.P. Zorzano (eds.), (World Scientific, Singapore, 2003), p.44.
- [18] D.N. Christodoulides and R.I. Joseph, Opt. Lett. **13**, 794 (1988).
- [19] D.N. Christodoulides, F. Lederer and Y. Silberberg, Nature (London) **424**, 817 (2003).
- [20] A. Trombettoni and A. Smerzi, Phys. Rev. Lett. **86**, 2353 (2001).
- [21] R. Morandotti, H.S. Eisenberg, D. Mandelik, Y. Silberberg, D. Modotto, M. Sorel, C.R. Stanley and J.S. Aitchison, Opt. Lett. **28**, 834 (2003).
- [22] R. Morandotti, D. Mandelik, Y. Silberberg, J.S. Aitchison, M. Sorel, D.N. Christodoulides, A.A. Sukhorukov and Yu.S. Kivshar, Opt. Lett. **29**, 2890 (2004).
- [23] D. Mandelik, R. Morandotti, J.S. Aitchison and Y. Silberberg, Phys. Rev. Lett. **92**, 093904 (2004).
- [24] R. Morandotti, H.S. Eisenberg, D. Mandelik, Y. Silberberg, D. Modotto, M. Sorel, C.R. Stanley and J.S. Aitchison, Opto-electronics review **13**, 103 (2005).
- [25] C. Raman, M. Kohl, R. Onofrio, D.S. Durfee, C.E. Kuklewicz, Z. Hadzibabic and W. Ketterle, Phys. Rev. Lett. **83**, 2502 (1999).
- [26] R. Onofrio, C. Raman, J.M. Vogels, J.R. Abo-Shaeer, A.P. Chikkatur and W. Ketterle, Phys. Rev. Lett. **85**, 2228 (2000).
- [27] S. Peil, J.V. Porto, B.L. Tolra, J.M. Obrecht, B.E. King, M. Subbotin, S.L. Rolston and W.D. Phillips, Phys. Rev. A **67**, 051603 (2003).
- [28] G. Theocharis, P. Schmelcher, P.G. Kevrekidis and D.J. Frantzeskakis, Phys. Rev. A **72**, 033614 (2005).
- [29] G. Theocharis, P. Schmelcher, P. G. Kevrekidis and D. J. Frantzeskakis, cond-mat/0509471.
- [30] H. Sakaguchi and B.A. Malomed Phys. Rev. E **72**, 046610 (2005).
- [31] R.S. MacKay and S. Aubry Nonlinearity **7** 1623 (1994).

- [32] G.L. Alfimov, V.A. Brazhnyi and V.V. Konotop, *Physica D* **194**, 127 (2004).
- [33] D.E. Pelinovsky, P.G. Kevrekidis and D.J. Frantzeskakis, *Physica D* **212**, 1 (2005).
- [34] E.J. Doedel, Lecture notice on “Numerical Analysis of Bifurcation Problems”, available at:  
<http://indy.cs.concordia.ca/auto/>
- [35] J.-C. van der Meer, *Nonlinearity* **3**, 1041 (1990).
- [36] M. Johansson and Yu.S. Kivshar, *Phys. Rev. Lett.* **82**, 85 (1999).



(c)

Figure 2: (a) Profiles of wave configurations and eigenfrequencies at the value of  $C = 0.1$  where the solid vertical line crosses branch one in the center diagram. Upper left: wave configuration from lower half of branch one,  $|1\rangle$ . Lower left: eigenfrequencies of the linearization around this solution. Upper right: Wave configuration from upper half of branch one,  $|1, e\rangle$ . Lower right: eigenfrequencies from the corresponding linearization. (b) Top: evolution of max square modulus of the solution taken from upper branch at  $C = 0.1$ . Middle: spatial profile of the square modulus of  $u$  taken for  $c = 0.1$ , after propagation by 250 units. Bottom: space time contour plot of the square modulus of the solution. (c) The top panel shows the most unstable eigenvalue of the two-site solution of  $|1, e\rangle$  as a function of the coupling strength  $C$ . The solid line is the full numerical result, while the dashed line denotes the analytical prediction. The bottom panel shows the correction for the central site  $n = 0$  and its neighboring site  $n = 1$  given by the first order theory (dashed line) versus the corresponding numerical result (solid line).

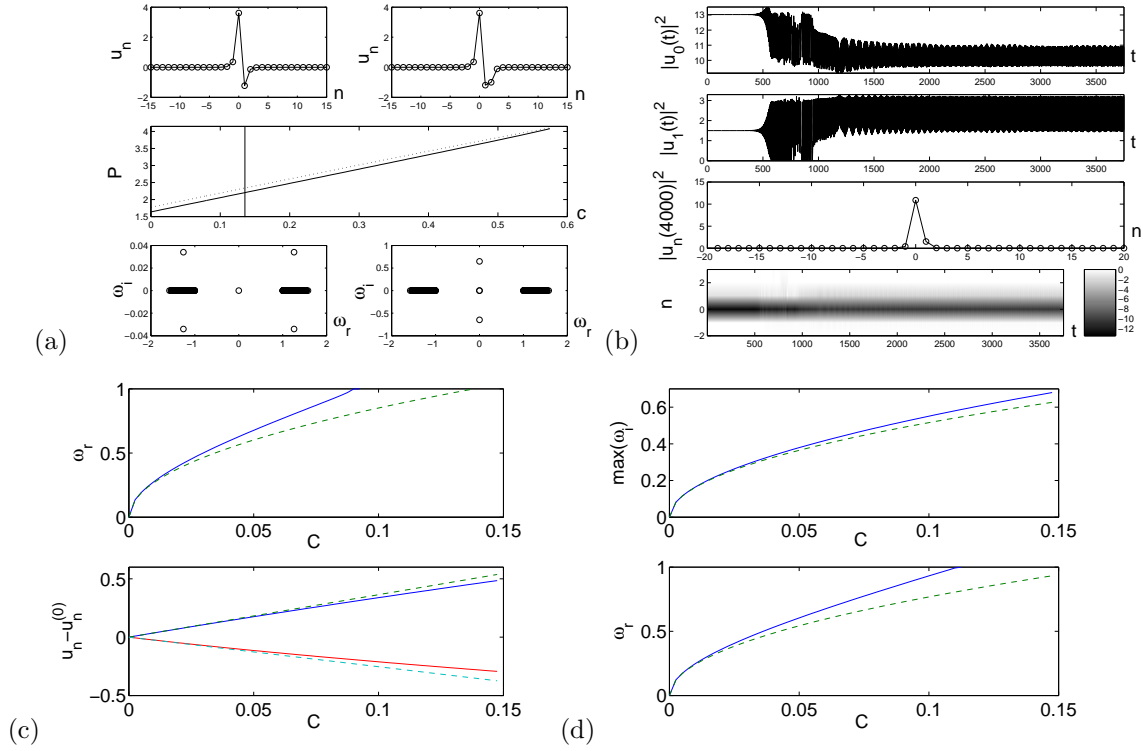


Figure 3: (a) Similar to Figure 2 for branch two with profiles at  $C = 0.135$ , for the branches  $|1, -e\rangle$  and  $|1, -e, -e\rangle$ . (a)-(c) are similar as above, while panel (d) shows the eigenfrequencies (one real and one imaginary, as predicted by theory) of the mode  $|1, -e, -e\rangle$  from the numerical results (solid) against the analytical predictions of section 2 (dashed lines).

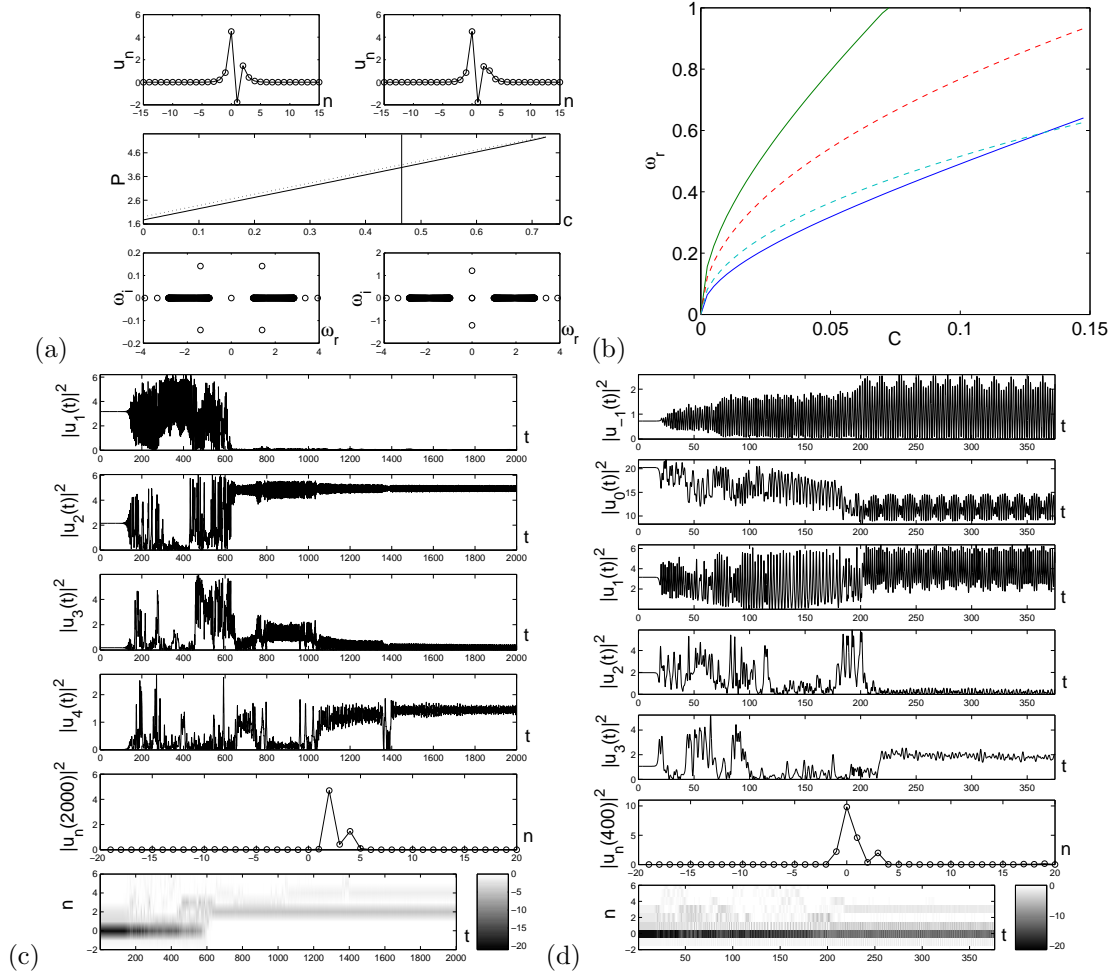


Figure 4: Panel (a) shows the profiles and eigenfrequencies of the third branch ( $|1, -e, e\rangle$  on the left and  $|1, -e, e, e\rangle$  on the right) for  $C = 0.465$ . The right panel shows, for the 3 site mode  $|1, -e, e\rangle$ , the dependence of its two eigenfrequencies against the analytical predictions (dashed lines). The bottom panels show, for each of the branches and for  $C = 0.465$ , the dynamical evolution of the principal sites, as well as the space-time contour plot of the square modulus.